Applied GIS

ISSN: 1832-5505
Vol-7 Issue-01 MAR 2019

Neural Control of Interconnected AC-DC Microgrids in Grid-Connected Hybrid Microgrids

B.ARUNA,ASSISTANT PROFESSOR, bonasiaruna@gmail.com

A.SABIHA,ASSISTANT PROFESSOR, asabiha.227@gmail.com

A.RAMEAH, ASSISTANT PROFESSOR, ramesh.andhala@gmail.com

Department of Electrical & Electronics Engineering, Sri Venkateswara Institute of Technology,

N.H 44, Hampapuram, Rapthadu, Anantapuramu, Andhra Pradesh 515722D

Abstract:

This study introduces an alternative approach to controlling the power flow of linked AC-DC microgrids in framework-associated mixed microgrids, which relies on implementing a modified combined interphase power regulator (UIPC). The investigated framework is a half-breed microgrid consisting of an alternating current (AC) microgrid and a direct current (DC) microgrid, as is typical in such systems. These microgrids are linked using an altered UIPC instead of the same linked power converters. This paper's main contribution is an adaptation of the conventional UIPC architecture that reduces the number of intensity converters used for power exchange regulation across AC-DC microgrids from three per stage to two. A line power converter (LPC) and a transport power converter (BPC) are two force converters that the revised design keeps in mind; the former controls the DC transport voltage and the latter remembers one for each stage. By connecting their DC transports to the LPCs, the AC microgrid is able to function in either capacitance mode (CM) or inductance mode (IM), and it is thus coupled with the main network. The LPCs' control architecture makes use of a fluffy rationale regulator. In order to reduce errors in the enrollment capacity structure, the fluffy derivation framework relies on a sophisticated H∞ sifting approach.The DC microgrid supplies the LPCs with DC electricity via the BPC. Regardless, the DC interface voltage of the LPCs is changing since a PV framework is providing the DC microgrid power in this situation. In light of this, another nonlinear disturbing affect on observer-based hearty variables is another later commitment to settle the DC connection variances.

The NDO-MS-SMC approach is used to regulate the BPC on the DC side. As an alternative to the current fuzzy controller, we also evaluate the system's reaction using a Neural Network controller. The suggested power stream control method of the upgraded UIPC for mixed microgrids is confirmed to be adequate by the recreation results.

I. INTRODUCTION

In the last decade, DC microgrids have allowed DC power assets like photovoltaic (PV)frameworks, energy units (FCs), energy storage systems (ESSs), and newly introduced DC loads like programmable DC electronic loads to become a part of the standard power grid [1]. However, AC microgrids allow for the connection of AC power assets (such as wind turbines) and AC loads (such as electrical engines) to the power systems [2-3]. Eventually, smart networks will coordinate AC and DC microgrids, which include both AC and DC power assets and loads, as a hybrid architecture known as half breed microgrids [4]. Power converters really link the alternating current and direct current microgrids. The microgrids are able to swap electricity with each other because to this relationship. In most cases, the force converters are linked in a way that increases the constant quality and trades a larger amount of intensity [5]. A typical, matrix-associated half-breed microgrid is shown in Fig. 1 as its structure. Pictured below are the DC microgrid components that make up a typical DC transport, including PV frameworks, ESSs, and associated loads [6]. Wind turbines, diesel generators, and AC loads are all possible

ISSN: 1832-5505
Vol-7 Issue-01 MAR 2019

components of an AC microgrid. One possible association with the forceframeworkorseparated is the whole half-and-half microgrid[8].Aside from that,The interlink power converters (ILCs) shown in Fig. 1 are used to link the basic transportation (joins) of two microgrids together [9]. However, as shown below [8-17], there are a number of specific challenges associated with modelling power converters in crossover microgrids:
- AMicrogrids are one-of-a-kind in many ways; for instance, they may alter their voltage, stage, frequency, and even their force.
- ASeveral microgrids may be combined to form a mixed microgrid. Think about it: there's one DC microgrid and two AC microgrids. Because the basic transports of the microgrids must have the same voltage greatness and period to avoid flowing current between equal associated ILCs, using them to trade power between microgrids in such a complex arrangement is complicated and troublesome.
- AEqually related ILCs with comparable force assessments must consistently distribute the moved force among microgrids.
- Modifications to the framework boundaries, such as line impedance, load variety, etc., impact the force sharing execution of the equal related ILCs.

Since a microgrid fault is a nonlinear event, the deficient current may be spread non-consistently across ILCs. In this case, the power that is exchanged could be drastically reduced since the current that is flowing through the force converters is expected to exceed the apparent current limitations of the converter. As a result, this can cause microgrid vulnerability or load concealment.
- AMicrogrids have oscillations in traded power and a great deal of uncertainty in produced power due to the intermittent behaviour of some distributed generation (DG) units.
- AHarmonics and other AC microgrid distortions generate a voltage loss due to a phase mismatch between individual load centres (ILCs) [15].
- AVarious power factors may be used by the interconnected ILCs in parallel. The power sharing performance is impacted by the voltage and power fluctuations caused by this.

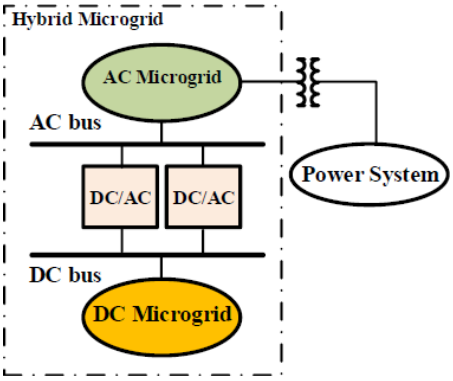

Fig.1.Atypicalgrid-connectedhybridmicrogrid

A plethora of written procedures and control mechanisms have been suggested to address the aforementioned difficulties.An equal-associated bidirectional ILC control system with many levels is suggested in [12].The fixed reference outline (SRF) has been used to create the cornerstone of the controls approach. Tomahawks did not share any terms and the review was harmonious. Because it is pre-structured in the SRF, this method is valuable because it is easy to implement. The main control level of the hang control-based varied levelled control approach that was suggested in [13] makes use of a hangplot.While the proportional-resonant (PR) regulator is used on the alternating current (AC) side, the comparable essential (PI) regulators are implemented on the DC side. The wave, generated by the main level of control, has been modified by the second level of control, and the utility and the crossover microgrid have been linked by the third level of control. For crossover microgrids that are part of a network, a vulnerability-secured dynamic force control scheme has been suggested in [14]. To differentiate between dynamic and responsive force movements, the method has made use of a configurable scalar. The authors of [15] demonstrated that force vacillations result from voltage imbalance. The current of each force converter was managed in order to modify the total of all ILC flows, as part of a suggested control strategy for parallel-connected ILCs. As a result, one of the ILCs has been deemed "excess" due to its high ratings. Because of this, the control plan is costly. Consonant bending is another area where the suggested method falls short, and the strategy likewise fails to reduce response force movements.A robust control plot for power sharing control between two equal related inverters has been designed in [16]. The present regulator of this procedure has been constructed using μ union examination.

ISSN: 1832-5505
Vol-7 Issue-01 MAR 2019

reversible power supplies. Two parallel-connected inverters may share power with the use of an ideal fragmented request regulator, as described in [17].The researchers in[18] have provided a blueprint for hybrid microgrids that adheres to IEEE 1547.4-2011. Within the confines of a microgrid, a decentralised and autonomous control system may be seen in [19]. A stronger control strategy is the result of the neighbourhood control activities that have been provided by the control strategy, which do not include correspondence joins. Power stream management in AC transmissionframeworks has also made use of the Flexible AC transmission System (FACTS) devices. This study introduces UIPC as a familiar tool for controlling the exchanged power across microgrids and as a basic foundation for a hybrid microgrid. Many force control applications with different control schemes have made use of the Realities devices. The united pressure stream regulator (UPFC) was used to improve voltage stability in [20]. Furthermore, the optimal UPFC fraction has been determined via genetic algorithms. Use of the between-line powerstream regulator (IPFC) to optimally manage the moving force in a transmission line was shown in [21]. Improve the forceframework security with monetary investigation by executing the static VAr compensators (SVCs), as described in [22]. A transmission line that links two territories in a force framework has the static simultaneous arrangement compensator (SSSC) applied to it [23]. When two territories have swapped possession of power, the SSSC has been a persuasive force. Initial presentation of the UIPC was in [24]. Using force converters instead of stage moving transformers at each stage, it is an improved version of the traditional IPC (interphase power regulator). In power stream control, the UIPC has been shown adequate in [24].

In a mixed microgrid scenario, this research focuses on small-scale modified UIPC to regulate the traded power across microgrids as the main network. These are the main things that this project will accomplish:

A half-and-half microgrid's core network and traded power may be managed using the UIPC instead of equal related power converters, which have several control concerns [8–17]. With this modification, power exchange control between AC-DC microgrids may be accomplished with a reduced number of intensity converters, as opposed to the three force converters used in the original UIPC design.The challenge of regulating the microgrids in a hybrid system arises because their components are different from the usual force framework components.

This study addresses the challenge of UIPC with a DC microgrid connected with its DC transport and introduces an additional control mechanism based on NDO-MS and SMC for the DC side of the BPC.As a result, this study focuses on UIPC as an alternative solution for controlling the flow of power across many microgrids in hybrid microgrids. There are a number of advantages of using UIPCs over more conventional equal associated power converters.

The ability to manage the power exchanged across microgrids without imposing cumbersome restrictions, such as similar voltage extents, stages, and so on, that are often required to connect the ILCs in a fair manner.

- AWithout resorting to an excess force converter, the UIPC may effectively limit the fault current, as shown in [24] and [15]. This component makes the connection more trustworthy, cheaply priced, and simpler compared to control approaches like the rapid force control plot that has traditionally been used for similar related ILCs.
- AAs shown in [24], the suggested modified UIPC provides a voltage confinement feature, even if there are equal linked ILCs that provide direct electrical links between microgrids.
- ALike the AC transport voltage, the DC transport voltage of a DC microgrid may be controlled by the UIPC. Use of the standard, equal-associated ILCs did not grant this trademark.

Therefore, in this study, a modified version of the UIPC is used to link half and half microgrids, achieving all the previously described characteristics. The rest of the paper is organised as follows: Section II shows the revised UIPC. To find the fluctuations of the usual DC transport voltage of the modified UIPC, Section III demonstrates an additional aggravating eyewitness based upon varied surface sliding mode control technique. In Section IV, we can see the outcomes of the contextual analysis and the results of the reproduction. Section V follows the completion of the task.

ISSN: 1832-5505
Vol-7 Issue-01 MAR 2019

II. PROPOSED UIPC BASED STRUCTURE OF HYBRID MICROGRID AND DYNAMIC MODELING

This section describes the proposed hybrid microgrid topology focused on the UIPC. The dynamic modelof the modified UIPC is also presented in thissection. Fig. 2 illustrates the studied hybridmicrogrid. As indicated, the grid-connected hybrid microgrid contains one AC microgrid and one DC microgrid which are interconnected through the UIPC. The AC microgrid, includes a diesel generator and related AC and DC loads. A PV system, abattery, and AC and DC loads exist in the DC microgrid. The loads, the PV system, and the battery are connected to the common DC bus (DC link).

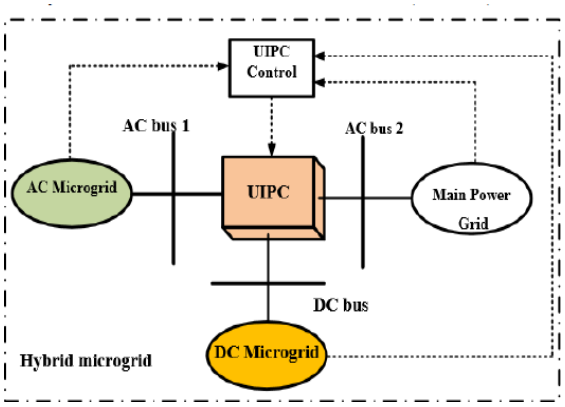

Fig. 2. Interconnection of AC-DC microgrids in grid-connected hybrid microgrid using UIPC

A. ConventionalUIPC

Figure 3 and the description of the UIPC's per-phase model may be found in [24]. Voltage source converters (VSCs) replaced the interphase power regulator's (IPC) phase-moving transformers in this setup. In this way, at each stage, three VSCs—including VSC1, VSC2, and VSC3—link two AC transports, say..1 and..2. Stage-moving converters VSC1 and VSC2 and voltage-controlling converter VSC3 are the three main functions of this circuit. Through transformer T1, VSC1 infuses the arrangement voltage into the line when operating in inductive mode.Once again, VSC2 operates in capacitive mode, infusing the line with the arrangement voltage..... via transformer T2. For instance, VSC3 regulates the AC voltage and is linked to one of the AC transports (here,..1) via transformer T3. All of the VSCs share a common capacitor that provides their DC transport. This way, the DC connection voltage..... is responsible for

rendering the dynamic forces of every VSC. Consequently, the exchanged power between the two AC transports may be adjusted using stage edge control of VSC1 and VSC2. In [24], you may find many nuances.

Figure 3. The conventional layout of the UIPC; three power converters are used in each phase. [24]

Section B: The UIPCC Workflow

We will start by making some changes to the traditional UIPC topology that we discussed in the last section. Next, in the part that follows, we will demonstrate the control strategy of the updated UIPC. The following issues plague the traditional UIPC layout, as seen in Fig. 3:

Since three VSCs are used in each phase, connecting three phases of AC buses requires nine VCSs and nine power transformers, which significantly increases the topology's cost.

- AAll of the VSCs in a given phase have their DC connections linked in tandem. According to [12, 25], however, when the output powers of the VSCs fluctuate or when there is a disturbance on the system model, such as a change in a system parameter, the common DC link voltage tends to oscillate among the VSCs having common DC connections. When VSCs share a DC connection, voltage fluctuations in that link pose a serious threat. In [24], this matter is not addressed.

Figure 4 shows the suggested improved UIPC model that would overcome the aforementioned obstacles. It can be seen that there is only one power converter used by each phase, denoted as $aPab$, where $b\in\{1,2,3\}$ represents the line number. The power converters inject the series voltage $Xyeb\prod\varphi ye=Xyef+aXyei$ onto each line, where $Xyef$ and $Xyei$ are the real and imaginary components of the injected series voltage, respectively. The impedance of the line

ISSN: 1832-5505
Vol-7 Issue-01 MAR 2019

$$S = V_2\left(\frac{V_1 - V_2}{Z_L}\right)^* = \quad (4)$$
$$(V_2\cos\delta_2 + jV_2\sin\delta_2)\frac{(V_1\cos\delta_1 + jV_1\sin\delta_1 - V_2\cos\delta_2 - jV_2\sin\delta_2)^*}{R_{L1} - jX_{L1}}$$

is ZLb=RLb+The majority of the time, the

In reality, the following is the general form of a controlled voltage source—injected series voltage:

$$V_{se} = K_A V_{DC}\angle K_P\varphi_{se}$$

where **N**A represents the phase coefficient and **N**o the voltage amplitude. The pulse width modulation (PWM) technique does affect the voltage amplitude coefficient KA, with the phase coefficient KP being around one and φye typically being equal to $\pi 2$. The injected voltage phase angle would coordinate the anti-parallel thyristor switches $S1$ and $S2$, which are controlled by the system. The sign of the phase angle determines which of these switches conducts at any given time for each phase. Whenever KP=+1, the UIPC is in the inductive mode (IM) and $S1$ is on while $S2$ is off.Similar to how $T1$ is off and $S2$ is on when the phasecoefficient KP equals -1, the UIPC is in capacitive mode (CM). Hence, the controllability of the power transferred between the two AC buses, $X1$ and $V2$, is possible. Additionally, you can see that all phases in Fig. 4 have a single BPC. After that, the DC microgrid is linked to the DC bus of this BPC. In order to control the AC voltage and exchange power with the DC microgrid, the BPC is linked to one of the AC buses (a weaker AC bus, also known as the AC microgrid bus) via transformer TBP**O**. In this case, it is $X1$. A look at Figure 5 reveals a vector representation of the system voltages taking into account the injected voltage of the proposed UIPC. It is possible to get the following from this diagram:

$$\varphi_{se}^{L} = \varphi_1 + \alpha_1$$
$$\varphi_{se}^{C} = \varphi_2 + \alpha_2$$

These angles are calculated by considering different operation modes of the UIPC, i.e. IM or CM. In Equations (2)-(3), $\varphi seL$and $\varphi seC$are the phase angle of the voltage at the middle point of the transmission line, when the UIPC operates in IM and CM modes, respectively.
According to complex power flow concept [26], the exchanged power between the two AC buses would be determined as follows:

where,$\delta 1$and$\delta 2$arethephaseanglesofthevoltages $V1$ and $V2$, respectively. After some mathematical manipulations, Equation (4) can be written asfollows:

ISSN: 1832-5505
Vol-7 Issue-01 MAR 2019

$$P = \frac{R_{L1}V_1V_2(\cos\delta_1\cos\delta_2+\sin\delta_1\sin\delta_2+R_{L1}V_2^2)-X_{L1}V_1V_2(\cos\delta_1\sin\delta_2-\sin\delta_1\cos\delta_2)}{{R_{L1}}^2+{X_{L1}}^2} \quad (5)$$

$$Q = \frac{R_{L1}V_1V_2(\cos\delta_1\sin\delta_2-\sin\delta_1\cos\delta_2)+X_{L1}V_1V_2(\cos\delta_1\cos\delta_2+\sin\delta_1\sin\delta_2+X_{L1}V_2^2)}{{R_{L1}}^2+{X_{L1}}^2} \quad (6)$$

Inmicrogrids,$RL1 \gg XL1$andweget:

$$P = \frac{V_1V_2(\cos\delta_1\cos\delta_2+\sin\delta_1\sin\delta_2+R_{L1}V_2^2)}{R_{L1}} = \frac{V_1V_2}{R_{L1}}(\cos(\delta_1-\delta_2)+R_{L1}V_2^2) \quad (7)$$

$$Q = \frac{V_1V_2(\cos\delta_1\sin\delta_2-\sin\delta_1\cos\delta_2)}{R_{L1}} = \frac{V_1V_2}{R_{L1}}\sin(\delta_2-\delta_1) \quad (8)$$

Thus, the transferred active power is controlled bythe voltage magnitudes of the AC buses whereas the reactive power is controlled by the phase angle difference. The voltage magnitude and phase angle difference are controlled by the proposed UIPC implying that the exchanged active and reactive powers between two AC buses would be controlled easily. Considering Fig. 6, to evaluate the effects of theinjectedvoltageoftheUIPC,andusingKirchhoff Voltage Law, we obtain:

$$V_1\angle\delta_1 - V_2\angle\delta_2 = (R_{L1}+jX_{L1})I + V_{se}\angle\varphi_{se} \quad (9)$$

Inthemicrogrids,$XL1P \cong RL1Q$andweget:

$$= (R_{L1}+jX_{L1})\frac{P-jQ}{V_2^r-jV_2^i} + \left(V_{se}^r + jV_{se}^i\right) =$$

Also,$RL1P \gg XL1Q$andwehave:

$$V_1\angle\delta_1 - V_2\angle\delta_2 = \left(\frac{V_2^r(R_{L1}P+X_{L1}Q)}{(V_2^r)^2+(V_2^i)^2} + V_{se}^r\right) + jV_{se}^i \quad (10)$$

The exchanged power between the DC link and the AC link (..1) can be obtained using the power balance equation as follows:

$$V_1\angle\delta_1 - V_2\angle\delta_2 = \left(\frac{V_2^r+V_{se}^r\left((V_2^r)^2+(V_2^i)^2\right)}{(V_2^r)^2+(V_2^i)^2}\right) + jV_{se}^i \quad (11)$$

$$V_{DC}I_{DC}^{UIPC} = \frac{3}{2}V_1^d i_1^d$$

where $IDCUIPC$is the current flowing in the DC link of the UIPC, and $V1d$ and $i1d$ are the d-axes voltage and current of the AC link, respectively.

Applied GIS

ISSN: 1832-5505
Vol-7 Issue-01 MAR 2019

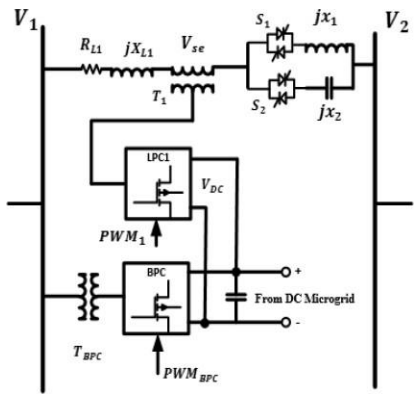

Fig. 4. Proposed topology of UIPC (each phase implements only one power converter, named asLPC)

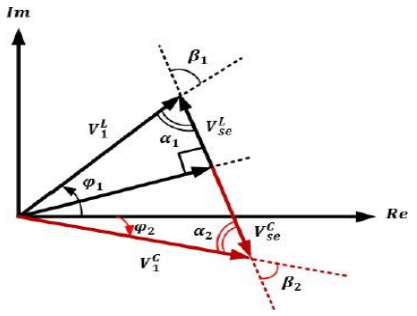

Fig.5.VoltageswhentheproposedUIPCisinvolved

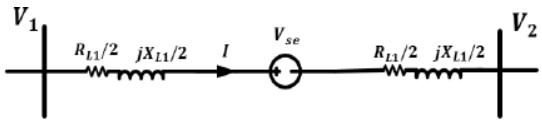

Fig. 6. Model of each phase of system considering injected voltage of proposed UIPC

Figure 7 shows the proposed per-stage geography of the linked microgrids in the cross-breed microgrid that are based on UIPC. This picture also shows the overall control structure of the UIPC that has been suggested. Two subsystems are part of the control framework: Series VSC control and DC connect control based on NDO-MS-SMC. A structure that utilises an ideal H∞based fuzzy reasoning regulator is employed by the Series VSC regulate subsystem to regulate the injected voltage and switches *S*1 and *S*2. The following section illustrates this control subsystem. An additional gravity-spectator-based hearty variable surface sliding mode control system is dependent on the SMC-

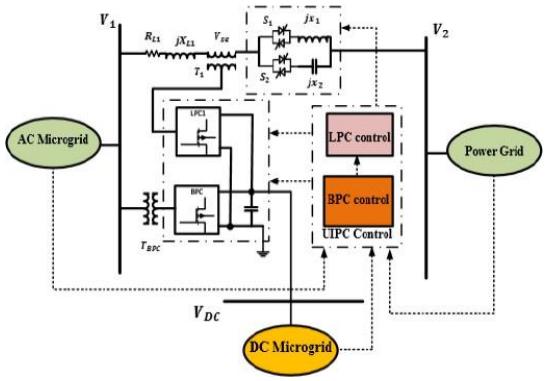

based DC connect control subsystem, which is responsible for stabilising the typical DC interface voltage fluctuations. The following region illustrates this control structure method.

A per-phase model of AC-DC microgrid connectivity using the UIPC and its control system is shown in Figure 7.
The suggested UIPC geography provides the following advantages over the conventional layout: - Each stage only requires one LPC. - The three-stage structure only requires one BPC.The overall model so requires four VSCs in addition to three force transformers.
- AIt is the DC microgrid that supplies the DC interface voltage. With this part, the UIPC may link the AC and DC microgrids.
- AThe LPCs' control structure makes use of an ideal fluffy reasoning regulator, which reduces the number of errors.
Section B: LPC Control Strategy
Both the LPCs control approach and the SMC based control scheme for the BPC are part of the proposed control conspire for the UIPC structure, as shown in Figure 7. Control cooperations are also present in these subsystems of control. The suggested method of controlling each LPCat step is shown in Figure 8. Line current and injected arrangement voltage are scaled and approximated, as shown. The next step is to use a bandpass channel to extract the important components of these scaled signals. The next section depicts the MATLAB-based resolution of the channel's boundaries (move work): - A disturbing impact

ISSN: 1832-5505
Vol-7 Issue-01 MAR 2019

eyewitness-based strong various surface sliding mode control approach is used to dampen the voltage fluctuations of the DC interface.

- .

ISSN: 1832-5505
Vol-7 Issue-01 MAR 2019

The next step is to calculate the filtered signals' rms values. The suggestion for the best fuzzy logic controller (FLC) is fed the injected voltage error. A PLL is used to measure the phase of the injected voltage. It is established that the UIPC functions in either IM or CM mode dependent on the sign of this phase, which is really KP in Equation (1). Because of this, the correct phase shift is used; $-\pi 2$ for CM mode and $+\pi 2$ for IM mode. In addition, the operating modes determine whether the switches $S1$ and $S2$ are active or disabled. The H∞ filtering design technique, which has been extensively detailed and verified in [28] by the authors of this study, is used to create the ideal FLC. Figure 8 shows how the control system for all LPCs receives a DC link voltage signal for coordination. An ideal FLC is then fed the erroneous signal. Based on these signals, the control signal (reference) is created for use in the PWM unit. Equation (1) explains how the injected voltage amplitude is regulated using the PWM system.

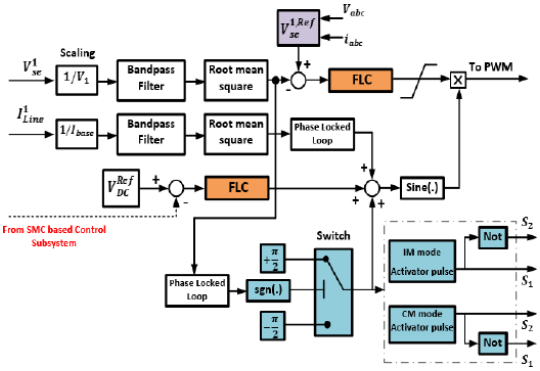

Fig.8.ProposedcontrolstrategyforLPCs

III. PROPOSED NDO MULTIPLE SURFACE SMC BASED DC LINK VOLTAGE CONTROL OF UIPC.

The DC links of the LPC and BPC are in parallel and connected to the common DC bus of the DC microgrid. As mentioned before, the DC link voltage would be unstable due to the output active power change of power converters, loads or PV system in the DC microgrid. Thus, a new NDO-MS-SMC is usedinthissectiontocontroltheDClinkvoltageof theproposed UIPC.

A.Structureofproposedcontrolscheme

Fig.9showstheproposedcontrolschemeforBPC.

In fact, and as described earlier, the BPC is responsible to regulate the DC link and therefore, the proposed scheme includes three parts: 1- the voltage control loop 2- the current control loop and 3- the NDO. The NDO is responsible for estimating the uncertainties and power changes in the DC microgrid.Furthermore, the NDO caters a reference signal for the dead-time compensation unit and the current control loop. The voltage control loop uses optimal proportional-integral(PI)controllersaccompaniedby the feedforward power disturbance to catch up the constitutional delay nested in the dynamics of the current control loop and the proposed disturbance observer. The PI controllers in both current and voltage control loops are optimally tuned using the genetic algorithm (GA).

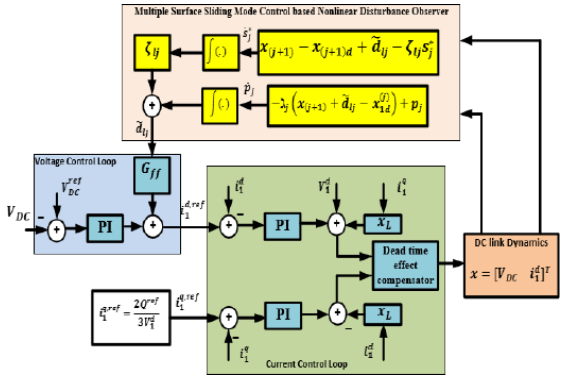

Fig. 9. Control of DC link of BPC based on new NDO-MS-SMC strategy

B.Dynamicmodelofnominalsystem

Firstly, the dynamic equations of the common DC link of BPC will be extracted without using any parametric uncertainty; so called the nominal model. Using Kirchhoff Current Law we get:

$$C\frac{dV_{DC}}{dt}=-I_{DC}^{UIPC}+I_{dist} \quad (14)$$

where, C is the capacitor of the common DC link,and $Idist=IDCPV+IESS+IL$ is the disturbancecurrent in which $IDCPV$ is the output DC current of the PV system, $IESS$ is the energy storage system (ESS) current (for example, a battery), and IL is the lumped DC loads current.

The BPC model in dq-frame can be expressed as follows [29]:

$$\begin{aligned} V_o^d &= V_1^d + L\frac{di^d}{dt} + \omega L i^q + i^d R \\ V_1^q &= L\frac{di^q}{dt} - \omega L i^d + i^q R \end{aligned} \quad (15)$$

ISSN: 1832-5505
Vol-7 Issue-01 MAR 2019

NDO-MS-SMC strategy isapplied to the BPC.AsshowninFig.9,theproposedcontrol { 0 dt 1 1

ISSN: 1832-5505
Vol-7 Issue-01 MAR 2019

Where, $Vo$and $V1$ are the output AC voltage of the BPC and AC bus to which the BPC is connected, respectively, ω is the angular frequency in rad/s, and L and R are the inductance and resistance of the output filter of the BPC, respectively.
Therefore, using Equations (12), (14), and (15) we obtain:

$$\begin{cases} \frac{dV_{DC}}{dt} = -\frac{3V_1^d i_1^d}{2CV_{DC}} + \frac{1}{C} I_{dist} \\ \frac{di_1^d}{dt} = \frac{V_o^d - V_1^d}{L} - \omega i_1^q - \frac{R}{L} i_1^d \end{cases}$$

Equation (17) indicates a system with nonlinear terms. This is the nominal model of the system.

C.Dynamicmodelofperturbedsystem
The uncertainties are considered on the capacitanceof the DC link C, the disturbance current, and the inductance L as follows:

$$\frac{1}{C} = \frac{1}{\bar{C}(1+\rho_C\theta_C)} = \frac{1}{\bar{C}} - \frac{\rho_C}{\bar{C}}\theta_C(1+\rho_C\theta_C)^{-1} \quad (18)$$

$$\frac{1}{L} = \frac{1}{\bar{L}(1+\rho_L\theta_L)} = \frac{1}{\bar{L}} - \frac{\rho_L}{\bar{L}}\theta_L(1+\rho_L\theta_L)^{-1} \quad (19)$$

$$I_{dist} = \bar{I}_{dist}\left(1+\rho_{I_{dist}}\theta_{I_{dist}}\right) \quad (20)$$

where, $\bar{C}$,$\bar{L}$,and$\bar{I}dist$ arethenominalvaluesofC,L, and$Idist$,respectively,andρC,ρL,and$\rho Idist$and θC, θL, and $\theta Idist$represent the probable perturbations on these parameters which are random numbers in the range of -1 to +1.

Introducing these perturbed parameters into the nominal system (17) we get:

$$\begin{aligned} \dot{x_1} &= \left(\frac{1}{\bar{C}} - \frac{\rho_C}{\bar{C}}\theta_C(1+\rho_C\theta_C)^{-1}\right)\left(-\frac{3V_1^d x_2}{2x_1}\right) \\ &+ \left(\frac{1}{\bar{C}} - \frac{\rho_C}{\bar{C}}\theta_C(1+\rho_C\theta_C)^{-1}\right)\left(\bar{I}_{dist}\left(1+\rho_{I_{dist}}\theta_{I_{dist}}\right)\right) \quad (21) \\ &= -\frac{3V_1^d x_2}{2\bar{C}x_1} + \frac{\bar{I}_{dist}}{\bar{C}} + \left(\frac{3V_1^d x_2}{2x_1}\right)\rho_C\theta_C(1+\rho_C\theta_C)^{-1} + \\ &\frac{\bar{I}_{dist}}{\bar{C}}\rho_{I_{dist}}\theta_{I_{dist}} - \frac{\bar{I}_{dist}}{\bar{C}}\rho_C\theta_C(1+\rho_C\theta_C)^{-1}\left(1+\rho_{I_{dist}}\theta_{I_{dist}}\right) \end{aligned}$$

$$\begin{aligned} \dot{x_2} &= \left(\frac{1}{\bar{L}} - \frac{\rho_L}{\bar{L}}\theta_L(1+\rho_L L)^{-1}\right)\left(-Rx_2 + u - V_1^d\right) - \omega i_1^q \quad (22) \\ &= \frac{R}{\bar{L}}x_2 + \frac{u}{\bar{L}} - \frac{V_1^d}{\bar{L}} - \omega i_1^q + \frac{\rho_L\theta_L}{\bar{L}}(Rx_2 - u + V_1^d)(1+\rho_L\theta_L)^{-1} \end{aligned}$$

D.DesignofNDO-MS-SMC

should be rewritten using the following disturbance parameters:

$$d_1(x,t) = \frac{I_{dist}}{\bar{C}} + \left(\frac{3V_1^d x_2}{2x_1}\right)\rho_C\theta_C(1+\rho_C\theta_C)^{-1} + \frac{\bar{I}_{dist}}{\bar{C}}\rho_{I_{dist}}\theta_{I_{dist}} - \frac{\bar{I}_{dist}}{\bar{C}}\rho_C\theta_C(1+\rho_C\theta_C)^{-1}\left(1+\rho_{I_{dist}}\theta_{I_{dist}}\right) \quad (23)$$

$$d_2(x,u,t) = -\omega i_1^q + \frac{\rho_L\theta_L}{\bar{L}}(Rx_2 - u + V_1^d)(1+\rho_L\theta_L)^{-1} \quad (24)$$

$d1(x,t)$isnamedasmatcheduncertaintywhereas $d2(x,u,t)$ is unmatched uncertainty, according to nonlinear control terminology [30]. Thus, the system is written in the following general standard form:

$$\dot{x}_n = a(x,t) + b(x,t)u(t) + d_n(x,u,t)$$

where,b=1$\bar{L}$.Thedisturbancein(25)iscontinuous

Step 2. Define the multiple surface sliding surfaces,as follows [30]:

$$s_j^* = s_j - s_j(0)e^{-\beta_j t}$$

$$s_j = x_j - x_{jd}$$

where, β is a positive constant value and xjd is the desired state trajectories. The purpose is to enforce each sliding surface $sj*$ to zero such that $xj \cong xjd$. Therefore, obtaining the derivative of the first sliding surfaces we have:

$$\dot{s}_1^* = \dot{s}_1 + s_1(0)\beta_1 e^{-\beta_1 t} = s_2 + x_{2d} + d_{l1} - \dot{x}_{1d}$$

The following procedures are followed in the design of the proposed NDO-MS-SMC, as shown in Figure 9, in this section:
First, establish the interrupted system model as the baseline:As a result, we have Equations (21), and (22).

Here is the definition of the estimation error:

Step 3: Create the real control rule The virtual control inputs have been developed up to this point; they are $x1d$ and $t2$. In order to bring the uncertain system (25) into stability, the following control input is suggested:

Thus, it follows that;

in where ζm is the switching gain, $\zeta l2$ is the

ISSN: 1832-5505
Vol-7 Issue-01 MAR 2019

linear gain, and the hyperbolic tangent function is about equivalent to:

is a small positive constant.By plugging in (32), the dynamic of the sliding surface $y2\prod$ may be expressed as:

ISSN: 1832-5505
Vol-7 Issue-01 MAR 2019

$$\dot{s}_2^* = -\zeta_{l2} s_2^* - \zeta_s sat(s_2^*)$$

Note that during obtaining the derivatives of the disturbances in the design procedure, the discrete control part had been excluded and did not appear in the derived equations. This is because whendesigning the SMC-based controller, the designed control signal contains two parts; the equivalent control energy $ueq$and a discrete part ud which is added to the obtained control signal to make it robust againstdisturbances.Noticethatduringdesigningthe controller and considering the disturbances, thedesign objective is to obtain the equivalent control energy law ueqbased on the Lyapunov energy function. Then, the discrete term ud is manually added to the control law to make the obtained signal robust. Therefore, the time derivative of the control lawexistsduring thedesignprocess.Formoredetails please refer to [33].

Step 4. Obtainingthedisturbance observerdynamics: The NDO aims to estimates the disturbance $\tilde{d}li$ as follows:

$$\begin{cases} \tilde{d}_{lj} = p_j + \lambda_j s_j^* \\ \dot{p}_j = -\lambda_j \left(s_{(j+1)} + x_{(j+1)d} + \tilde{d}_{lj} - x_{1d}^{(j)} \right) \end{cases} \quad -(35)$$

where, pj and λj are a dummy variable and gains of the observer, respectively. Calculating the derivative of $\tilde{d}$ lj we get:

$$\dot{\tilde{d}}_{lj}^{(1)} = \dot{p}_j + \lambda_j \dot{s}_j^* = -\lambda_j \left(s_{(j+1)} + x_{(j+1)d} + \tilde{d}_{lj} - x_{1d}^{(j)} \right) + \lambda_j \left(s_{(j+1)} + x_{(j+1)d} + d_{lj} - x_{1d}^{(j)} \right) = \lambda_j (d_{lj} - \tilde{d}_{lj}) = \lambda_j e_{d_{lj}} \quad (36)$$

and;

$$\|\dot{d}_l\| \le \gamma \quad (37)$$

Step 5. Stability proof: The Lyapunov function is defined as:

$$V_1(e_{d_l}) = e_{d_l}{}^T P e_{d_l}$$

Calculating the derivative of Lyapunov function and using Equations (34)-(36) we get:

$$\dot{V}_1 = e_{d_l}{}^T (D^T P + PD) e_{d_l} + 2 e_{d_l}{}^T P \dot{d}_l \le -e_{d_l}{}^T Q e_{d_l} + 2\|e_{d_l}\| . \|P\| . \|\dot{d}_l\|$$

where, $D = diag[\lambda \quad \lambda]$ Q is a positive arbitrary matrix, and P is a positive matrix such that the following constraint is satisfied.

$$D^T P + PD = -Q \quad (40)$$

Analytically:

$$P = \begin{bmatrix} P_{11} & P_{12} \\ P_{12}^T & P_{22} \end{bmatrix} \quad (41)$$

and we have:

$$\begin{bmatrix} \lambda_1 & 0 \\ 0 & \lambda_2 \end{bmatrix} \begin{bmatrix} P_{11} & P_{12} \\ P_{12}^T & P_{22} \end{bmatrix} + \begin{bmatrix} P_{11} & P_{12} \\ P_{12}^T & P_{22} \end{bmatrix} \begin{bmatrix} \lambda_1 & 0 \\ 0 & \lambda_2 \end{bmatrix} = -Q \quad (42)$$

Therefore, considering Q as an identical matrix, and using (30) and (35)-(37), e_{d_l} will be bounded by;

$$\|e_{d_l}\| \le \lambda_l \quad (43)$$

where;

$$\lambda_l = \frac{2\|P\|\gamma}{\lambda_m} \quad (44)$$

and the system is robustly stable.

IV. NEURALNETWORK:

These days, it's more common to talk of "artificial neural networks" made up of "nodes" rather than "neurons" when discussing networks of neurons.[1]The two main types of neural networks used to solve AI challenges are abiological networks, which consist of actual biological neurons, and artificial neural networks. The weights represent the connections of the real neuron. If the weight is positive, then the connection is excitatory, and if it is negative, then the link is inhibitory. Each input is given a weight and then added together. We call this action a linear combination. Activation functions are used to regulate the output amplitude in the end. As an example, the typical permissible range of output is from 0 to 1, although it might also be between -1 and 1. Predictive modelling, adaptive control, and other applications that allow for dataset training are all possible with these artificial networks. Networks are capable of self-learning via experience and may draw inferences from complicated and apparently unrelated data sets.

ISSN: 1832-5505
Vol-7 Issue-01 MAR 2019

Fig. 10 Simplified view of a feed-forward artificial neural network

Artificialintelligence:

Networks of real or artificial neurons linked together in a scientific or computational model for data preparation based on a connectionistic approach to computation make up what is known as a neural system (NN), which is short for "fake neural system" (ANN) or "imited neural network" (SNN). In most cases, an ANN is a flexible framework whose structure changes in response to inputs flowing into or out of the system.

Neural systems are more accurately described as dynamic tools that show non-straight factual information. They may be used to highlight intricate relationships between data sources and results or to unearth hidden patterns in data. The connections between the handling components and component borders allow a counterfeit neural system to display complicated global behaviour. This behaviour is shown by a system of simple preparing components, known as fake neurons.Warren McCulloch, a neurophysiologist, and Walter Pitts, a rationalist, first collaborated at the University of Chicago; they first postulated fake neurons in 1943.

The repeating Hopfield architecture is an example of a more traditional kind of artificial neural network. The concept of a neural network seems to have originated with Alan Turing, who referred to them as "B-type chaotic machines" in his 1948 article Intelligent Machinery.

The ability to derive a capability from perceptions and then put it to use is what makes fake neural system models useful. The remarkable qualities of information appropriation can be captured by unaided neural systems through learning representations of the data (e.g., the Boltzmann machine (1983)) and, more recently, by deep learning calculations, which can indeed become proficient with the data's dissemination capacity. When human planning of such capacity is impractical due to the unpredictability of the data or task, neural network learning becomes invaluable. Possible uses:

Neural networks have many potential applications. The tasks that counterfeit neural systems are

used often fall under the following broad categories:

• Time arrangement expectation and display, as well as function estimation or relapse evaluation.
• Categorization, which encompasses example and grouping identification, anomaly detection, and sequential tracking.
Sifting, grouping, dazzle signal partitioning, and pressure are all aspects of data processing. Applicationareas of artificial neural networks that use nonlinear framework identification [19] from dynamic and game-playing domains (e.g., chess, backgammon, and dashing) to design and grouping domains (e.g., motion, discourse, and transcribed content), clinical conclusion, financial applications, information mining (or information revelation in databases, "KDD"), perception, and email spam sifting. One example is the possibility of creating a semantic profile of the client's preferences using images that have been trained for object recognition.
In the realm of neuroscience, the subfield known as "hypothetical and computational neuroscience" is concerned with the computer modelling and theoretical investigation of potential brain networks. The field is strongly associated with psychological and social characteristics, since neural frameworks are individually linked to intellectual operations and behaviour.
The goal of this area of study is to understand the inner workings of organic frameworks by creating models of natural brain networks. Neuroscientists try to glean this knowledge by establishing a link between observed natural processes (information), biologically plausible tools for brain processing and learning (organic neural system models), and hypotheses (data hypothesis and factual learning hypothesis).
Category of models
Several models are used, each with its own level of discussion and representation of a different component of a neural network. Models of behaviour arising from conceptual brain modules that speak to completion follow models of the transient conduct of individual neurons and models of the components of

ISSN: 1832-5505
Vol-7 Issue-01 MAR 2019

neural hardware resulting from cooperations between individual neurons.

underlying components. This includes models of the long-term and short-term plasticity of neural networks, as well as their relationship to learning and memory at both the neuronal and network levels.

V. SIMULATIONRESULTS:

a. WithConventionalcontroller:

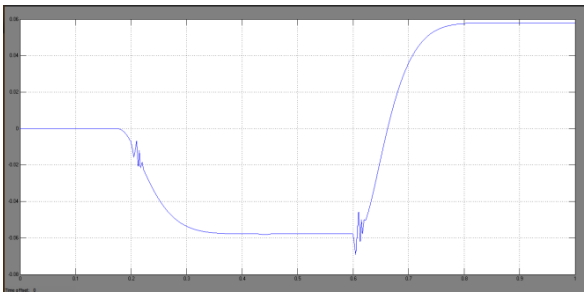

Fig.11.VSESeriesInjectedVoltage

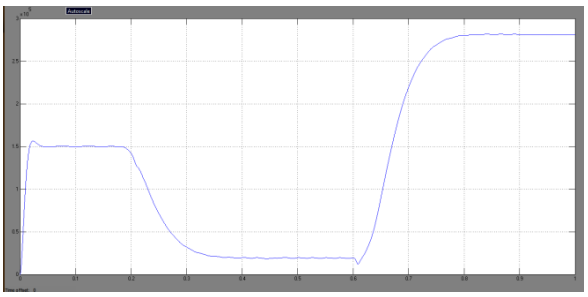

Fig.12.PseInjected Power

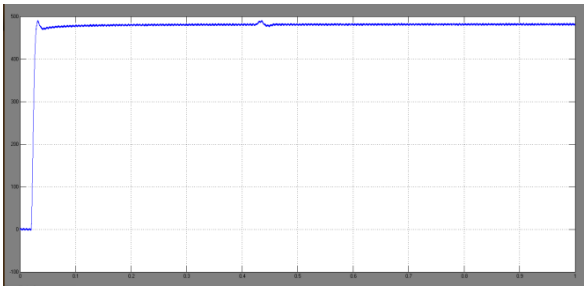

Fig.13.DcLINK VOLTAGE

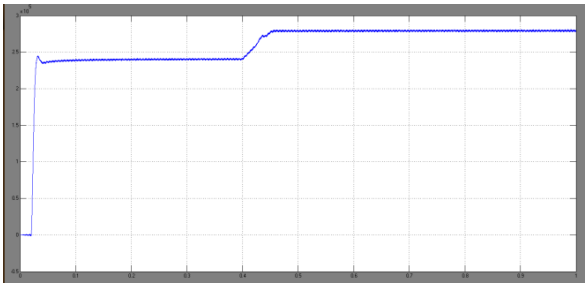

Fig.14.ActivepowerofDClinkwhen40kWis demanded from the AC side

ISSN: 1832-5505
Vol-7 Issue-01 MAR 2019

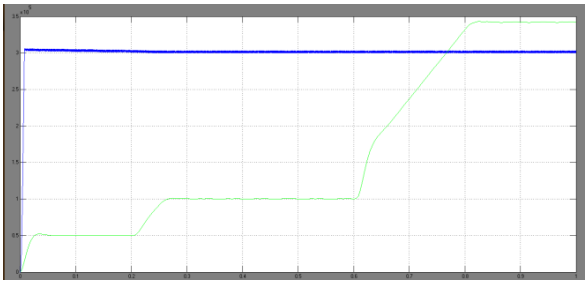

Fig.15.Generationineachmicrogrid

b. Simulation results with Neural Nework Controller:

Fig.16.VSESeriesInjectedVoltage

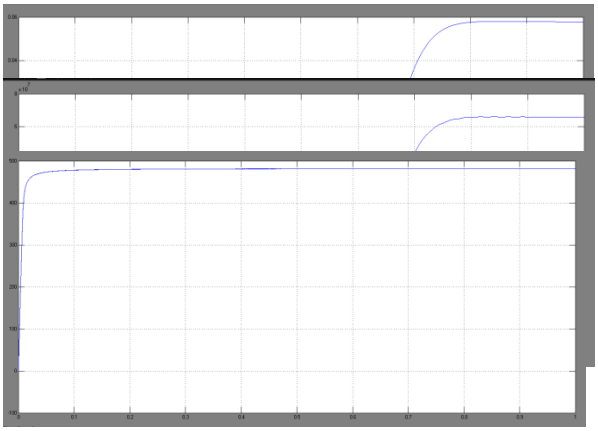

Fig.17.PseInjected Power

Fig.18.DcLINK VOLTAGE

ISSN: 1832-5505
Vol-7 Issue-01 MAR 2019

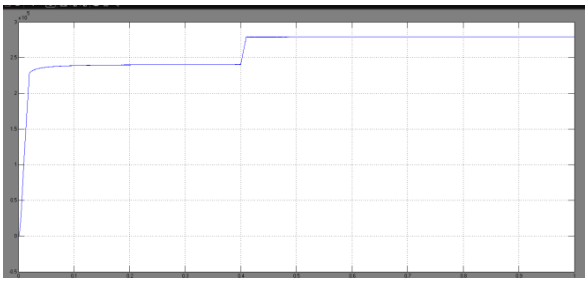

Fig.19.ActivepowerofDClinkwhen40kWis demanded from the AC side

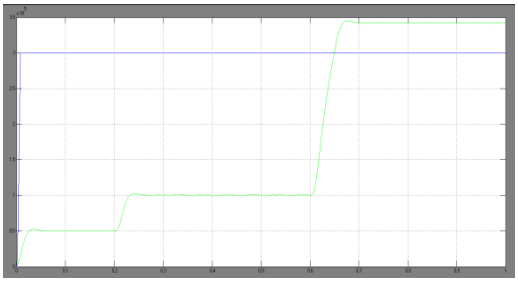

Fig.20.Generationineachmicrogrid

VI. CONCLUSION:

The most likely future smart grid architecture for integrating renewable resources and AC/DC loads is the hybrid microgrid. The reason for this is because this structure has the best features of both AC and DC microgrids all at once. The power exchange control between linked AC and DC microgrids is a common issue with this design. Instead of using the problematic parallel-connected power converters, this research suggests a UIPC based solution. Before introducing effective control measures for the revised UIPC, a revised structure for the UIPC was initially suggested. The updated model and the performance of power exchange regulation between AC and DC microgrids were both confirmed by the simulation results. When compared to a fuzzy logic controller, a Neural Network controller improves the system's performance.

VII. REFERENCES

[1] Runfan Zhang, Branislav Hredzak, "Distributed Finite-Time Multi-Agent Control for DC Microgrids with Time Delays", IEEE Transactions on Smart Grid, Early Access, 2018.

[2] Kumar Utkarsh, et al, "Distributed Model-predictiveReal-timeOptimal Operationofa Network ofSmartMicrogrids",IEEETransactionsonSmart Grid, Early Access, 2018.

[3] Haifeng Qiu, et al, " Bi-level Two-stage Robust Optimal Scheduling for AC/DC Hybrid Multi-microgrids",IEEETransactions on SmartGrid,Early Access, 2018.

[4] Pengfeng Lin, et al, "A Distributed Control Architecture for Global System Economic Operation in Autonomous Hybrid AC/DC Microgrids", IEEE Transactions on Smart Grid, Early Access, 2018.

[5] Daniel E. Olivares, et al, "Trends in Microgrid Control", IEEE Transactions on Smart Grid Volume: 5, Issue: 4, pp. 1905 – 1919, 2014.

[6] Jongwoo Choi, et al, "Robust Control of a Microgrid Energy Storage System using Various Approaches", IEEE Transactions on Smart Grid, Early Access, 2018.

[19] Huanhai Xin, et al., "A Decentralized Hierarchical Control Structure and Self-Optimizing Control Strategy for F-P Type DGs in Islanded Microgrids", IEEE Transactions on Smart Grid, Volume: 7, Issue: 1, pp. 3 – 5, 2016.

[20] Priyank Srivastava, Rashmi Pardhi "A Review onPowerSystemStabilityandApplicationsofFACT Devices" International Journal of Engineering Research and Applications, Volume: 3, Issue: 3, pp.879-883, 2013.

[21] Akanksha Mishra and G.V. Nagesh Kumar, "Congestion Management of Power System with InterlinePowerFlowControllerUsingDisparityLine Utilization Factor and Multi-objective Differential Evolution" CSEE Journal of Power and Energy Systems, Volume: 1, Issue: 3, pp. 76 - 85 2015.

[22] B. Vijay Kumar, et al., "Optimization of UPFC location and capacity to improve the stability using ABC and GSA algorithm", IEEE, Power and Energy Conference at Illinois (PECI), 2015.

[23] K.K. Sen, "SSSC-static synchronous series compensator: theory, modeling, and application", IEEE Transactions on Power Delivery, Volume: 13, Issue: 1, pp. 241 - 246 ,1998.

[24] J. Pourhossein, et al., "Unified Interphase Power Controller(UIPC)ModelingandItsComparisonwith IPC and UIPFC", IEEE